X-ray Photoelectron Spectroscopic Studies of Carbon Fiber Surfaces. 13. Valence-Band Studies of Oxidized Fibers Interpreted by Xα Calculations

Yaoming Xie and Peter M. A. Sherwood*

Department of Chemistry, Willard Hall, Kansas State University, Manhattan, Kansas 66506

Received August 3, 1990. Revised Manuscript Received November 6, 1990

The results of valence-band X-ray photoelectron spectroscopy (XPS) of oxidized carbon fibers are interpreted by Xα calculations on model compounds based upon oxidized coronene fragments. The results indicate that valence-band XPS can distinguish between ether/epoxide and hydroxide surface functionality and that the valence-band region is potentially more sensitive to differences in surface functionality than the core region. XPS data for quinone and hydroquinone with the valence-band region interpreted by Xα calculations are presented and related to the carbon fiber spectra.

Introduction

We have carried out a series of studies on the nature of untreated and oxidized carbon fiber surfaces[1-13] in order to understand the surface functionality of these important materials. In particular these studies allows us to obtain a better appreciation of how surface functionality is related to composite properties, which is especially important due to the expanding applications of composites-containing carbon fibers.

Many of our previous studies have involved X-ray photoelectron spectroscopy (XPS) and X-ray diffraction (XRD). These two techniques allow information to be obtained about the surface and bulk chemistry of these materials. In XPS studies the bulk of the work has concentrated upon the core region, but recently we[10-13] have been interested in the valence-band region and have shown it to reveal a greater sensitivity to chemical change than the core regions.

The purpose of this paper is to compare the valence-band spectra of oxidized pitch-based fibers with calculated valence band spectra obtained by Xα calculations. The calculations allow for a general understanding of the features that may be found on oxidized fibers and thus enhance the analytical application of valence-band XPS to such materials.

Experimental Section

Du Pont E-120 untreated and unsized carbon fibers were electrochemically oxidized by using a nitric acid electrolyte at various potentials (vs the saturated calomel electrode (SCE)). Full details of these treatments are given elsewhere.[13] The treatment was potentiostatic for 20 min. Most commercial treatment methods use galvanostatic treatment for much shorter time periods. We will discuss the effects of galvanostatic treatment and electrostatic treatment and the effect of treatment time in a later publication. Hydroquinone and quinone samples were purchased from Alpha and were of analytical grade quality.

The X-ray photoelectron (XPS or ESCA) spectra were collected on an AEI (Kratos) ES200B X-ray photoelectron spectrometer with a base pressure of about 10^{-9} Torr. The spectrometer was operated in the FRR mode (ratio 1:23) using Mg $K\alpha_{1,2}$ X-ray radiation (240 W). Analyzer resolution was of the same order as the X-ray line width (0.7 eV). Typical data collection times were as follows: C(1s), 1 h; O(1s), 10 H; valence band, 16–24 h. There was a little decomposition observable for long data collection times in the valence-band region.[13] The spectrometer energy scale was calibrated by using copper,[14] and the separation (233 eV) between photoelectron peaks generated by Mg and Al $K\alpha_{1,2}$ X-rays.

A bundle of carbon fibers was cut to a length of 3.0 cm, with both ends tied with a narrow piece of aluminum foil. One of the ends was mounted in a metal sample holder. After insertion into the XPS spectrometer chamber, the sample was connected to the system ground by the metal sample holder. The position of the sample holder was adjusted so that no photoelectrons were seen from the same holder and the aluminum foil. The hydroquinone and quinone spectra were taken by examining the powders at liquid nitrogen temperatures.

The curve fitting of the XPS spectra was carried out using a nonlinear least-squares curve-fitting program with a Gaussian/Lorentzian product function.[15,16] The Gaussian/Lorentzian mix was taken as 0.5, except for the "graphitic" carbon peak, which was taken as 0.84 with an exponential tail. These values for the Gaussian/Lorentzian mix were chosen after many studies were carried out where the Gaussian/Lorentzian mix was varied to ensure the best fit to various types of C(1s) component peak.[1-13] The C(1s) binding energy of the graphitic peak was taken as 284.6 eV for calibration purposes.

Multiple-scattered wave Xα calculations were performed on an IBM Personal System/2 computer Model 80 using highly otimized double-precision Fortran code with the processor operating in 32-bit mode running under XENIX. Table I shows the input parameters and calculation features for the six model compounds studied. The parameters for the substituted coronenes are similar to those chosen for coronene in our earlier paper[10] (Table V of ref 10 shows sphere radii for carbon and hydrogen in angstroms, when they were actually given in atomic units; the maximum l value for carbon should also have been shown as 1 and not 2). Ground-state calculations were performed for the substituted coronenes due to the large number of levels involved

(1) Proctor, A.; Sherwood, P. M. A. *J. Electron Spectrosc.* **1982**, *27*, 39.
(2) Proctor, A.; Sherwood, P. M. A. *Carbon* **1983**, *21*, 53.
(3) Proctor, A.; Sherwood, P. M. A. *Surf. Interface Anal.* **1982**, *4*, 212.
(4) Kozlowski, C.; Sherwood, P. M. A. *J. Chem. Soc., Faraday Trans. 1* **1984**, *80*, 2099.
(5) Kozlowski, C.; Sherwood, P. M. A. *J. Chem. Soc., Faraday Trans. 1* **1985**, *81*, 2745.
(6) Harvey, J.; Kozlowski, C.; Sherwood, P. M. A. *J. Mater. Sci.* **1987**, *22*, 1585.
(7) Kozlowski, C.; Sherwood, P. M. A. *Carbon* **1986**, *24*, 357.
(8) Kozlowski, C.; Sherwood, P. M. A. *Carbon* **1987**, *25*, 751.
(9) Xie, Y.; Sherwood, P. M. A. *Appl. Spectrosc.* **1989**, *43*, 1153.
(10) Xie, Y.; Sherwood, P. M. A. *Chem. Mater.* **1989**, *1*, 427.
(11) Xie, Y.; Sherwood, P. M. A. *Chem. Mater.* **1990**, *2*, 293.
(12) Xie, Y.; Sherwood, P. M. A. *Appl. Spectrosc.* **1990**, *44*, 797.
(13) Xie, Y.; Sherwood, P. M. A. *Appl. Spectrosc.*, in press.
(14) Annual Book of ASTM Standards, Vol. 03.06; in *Surf. Interface Anal.* **1988**, *11*, 112.
(15) Sherwood, P. M. A. *Practical Surface Analysis by Auger and Photoelectron Spectroscopy*; Briggs, D., Seah, M. P., Eds.; Wiley: London, 1983; Appendix 3.
(16) Ansell, R. O.; Dickinson, T.; Povey, A. F.; Sherwood, P. M. A. *J. Electroanal. Chem.* **1979**, *98*, 79.

0897-4756/91/2803-0164$02.50/0

Table I. Parameters Used and Features of the Xα Calculations

α values	carbon, 0.75928; hydrogen, 0.77654; oxygen 0.74447					
max l value	outer 4, carbon 1, oxygen 1, hydrogen 0					
cluster	$C_{24}O_{12}$	$C_{24}O_{12}H_{12}$	$C_{24}O_{12}H_6$	$C_{24}O_6$	$C_6O_2H_4$	$C_6O_2H_6$
sym	D_{6h}	D_{6h}	D_{6h}	D_{6h}	D_{2h}	C_{2h}
outer-sphere α value	0.754 34	0.759 89	0.757 51	0.756 32	0.762 56	0.764 56
inner-sphere α value	0.754 34	0.759 89	0.757 51	0.756 32	0.762 56	0.764 56
C–C bond lengths, Å	1.4200	1.4200	1.4200	1.4200	1.322, 1.477	1.390, 1.380
C–O bond lengths, Å	1.2150	1.3500	1.2825	1.4200	1.222	1.400
O–H bond lengths, Å		0.9600	1.4750		1.000[c]	1.000[c], 0.920
carbon-sphere radius, Å						
central ring	0.820	0.820	0.820	0.820	0.764[a]	0.785[a]
closest C to central ring	0.821	0.817	0.820	0.788	0.806[b]	0.806[b]
outer carbon atoms	0.770	0.799	0.786	0.827		
hydrogen sphere radius, Å		0.370	0.695		0.450	0.450
oxygen sphere radius, Å	0.831	0.814	0.840	0.788	0.817	0.806
outer sphere radius, Å	5.752	6.358	6.342	5.082	3.463	3.733
virial ratio ($-2T/V$)	1.017 89	1.022 71	1.018 75	1.022 39	1.016 21	1.019 72

convergence When the difference in potentials at the beginning and end of the iteration were less than 10^{-5} of the potential at the start of the iteration. This gives energy levels that differed by less than 10^{-6} Rydbergs between the last two iterations. Core electrons: "thawed" so that they retained atomic character while being fully included in the iterative process. C(1s) and O(1s) electrons were treated as core electrons.

[a] Carbon atom attached to O or OH. [b] C–H carbon atoms. [c] C–H bond distance.

and the similarity between the relative transition-state and ground-state values that we have found for hydroquinone and quinone (which suggests that a full set of transition-state calculations might not give much difference from the ground-state data). Hydroquinone and quinone had a full set of transition-state calculations performed for all the valence energy levels. The calculated spectra were obtained by weighting the atomic contributions to the molecular orbitals with the Scofield cross sections.[17] The component energy levels were made up of equal-width Gaussian/Lorentzian product functions with a 50% mix (the same function used for fitting the spectra) including X-ray satellite features for the Mg X-radiation used in the experimental spectra. Variation in the width of the levels might change some spectral features, but there is no justification for doing this.

Results and Discussion

Figure 1 shows the calculated valence-band spectrum together with a drawing of the model compounds. These spectra reveal two main features:

(i) The separation between the highest binding energy peak due to O(2s) intensity (around 30 eV) and the peak due to C (2s) intensity (around 20 eV) decreases steadily from the model compound with epoxide functionality, the oxide functionality compound, the "hydrogen bridged" compound, and the hydroxide compound. This is particularly interesting since epoxide and hydroxide functionality (identical in the O(1s) region) can be clearly distingushed and the oxide and hydroxide O(2s) features are reversed with respect to their O(1s) region positions (where the oxide O(1s) feature has a lower binding energy than the hydroxide feature). It should be noted that the actual separation depends upon the oxygen-to-carbon ratio, since we are considering the separation between the O(2s) peak and a C(2s) "composite peak". This "composite peak" is made up of the overlap of a number of component peaks so that its actual position will depend upon the relative oxygen to carbon cross sections. We discuss below how we vary these cross sections to represent carbon fiber surfaces with different oxygen-to-carbon ratios. It can be seen that the separation between the O(2s) and the first C(2s) feature steadily decreases in the series (6.74, 4.00, 2.59, and 2.27 eV) while that of the "composite peak" maximum decreases a little less markedly (10.58, 8.92, 8.85, and 8.77 eV). The hydroxide-substituted coronene shows a distinct feature at a separation of 5.45 eV, and the "bridged structure" shows a weak feature at a separation of 5.85 eV. Comparison of the spectra in Figure 1 with

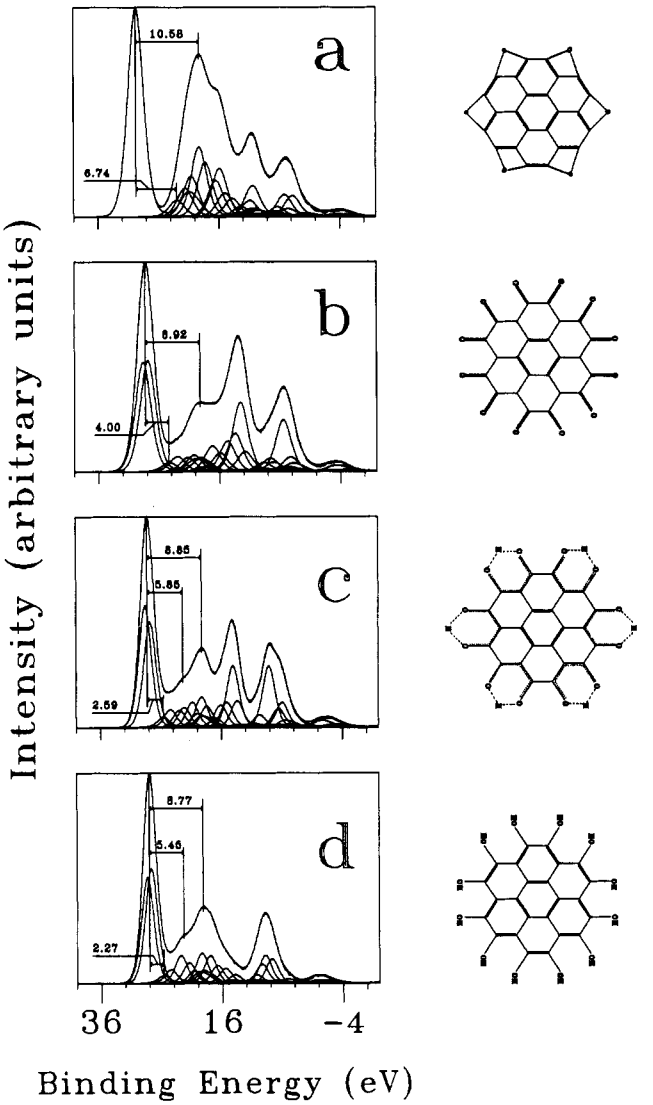

Figure 1. Spectra of model compounds generated from the Xα calculations: (a) epoxide-group-substituted coronene; (b) oxide-group-substituted coronene; (c) hydrogen-bridged oxide-substituted coronene; (d) hydroxide-group-substituted coronene.

(17) Scofield, J. H. *J. Electron. Spectrosc.* **1976**, *8*, 129.

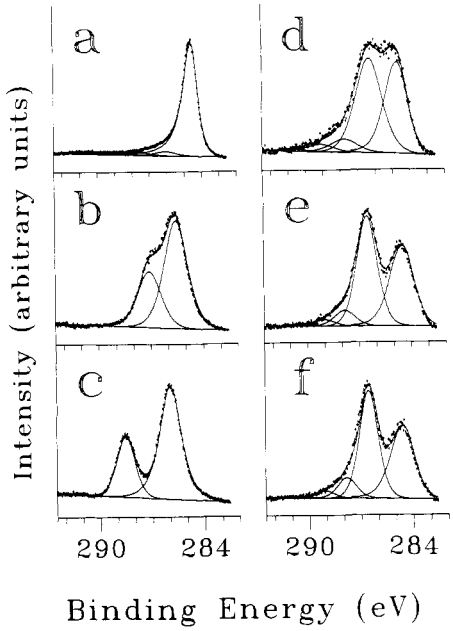

Figure 2. C(1s) region XPS spectra of various carbon fiber samples and hydroquinone and benzoquinone: (a) untreated E-120 carbon fiber; (b) solid hydroquinone condensed onto a liquid nitrogen cooled sample probe; (c) solid benzoquinone condensed onto a liquid nitrogen cooled sample probe; (d) E-120 carbon fiber anodically oxidized at 2.0 V (SCE) for 20 min; (e) E-120 carbon fiber anodically oxidized at 2.5 V (SCE) for 20 min; (f) E-120 carbon fiber anodically oxidized at 3.0 V (SCE) for 20 min.

those in Figure 5 where the oxygen cross section is reduced shows how the "composite peak" features change.

(ii) A distinct "signature" is notable in the region below 18-eV binding energy. This "signature" is made up of the overlap of various different peaks and can be shown to change as the amount of oxygen and carbon in the compound varies.

To evaluate whether our prediction in (i) was reasonable, we obtained the valence-band spectrum of quinone and hydroquinone and interpreted these spectra with Xα calculations.

We have suggested on several previous occasions[5,8,11] that electrochemical oxidation can, under appropriate conditions, produce a surface-oxidized state that corresponds to a "bridged structure" similar to that for the model compound $C_{24}O_{12}H_6$ shown in Figure 1c. We have based this suggestion on the fact that the C(1s) chemical shift for the carbon attached to the oxygen atom of the bridge has a shift between that of a typical >C=O group and a typical >C–OH group. Thus in Figure 2 it can be seen that the C(1s) region of hydroquinone (Figure 2b) shows a distinctly smaller shift than that for quinone (Figure 2c)—in both cases the spectrum is fitted to an intensity ratio of 1:2 as expected. The typical C(1s) region for an untreated fiber (Figure 2a) changes to show chemically shifted features corresponding to hydroxide (2.0 V vs SCE, Figure 2d) and at more oxidizing potentials (2.5 V vs SCE, Figure 2e, and 3.0 V vs SCE, Figure 2f) a peak intermediate between the typical hydroxide peak (Figure 2b) and the typical oxide peak (Figure 2c). There is also a single relatively narrow O(1s) feature corresponding to this type of functionality,[13] which excludes the possibility of a nonsymmetrical ketol structure since such a structure would have two different types of oxygen (—OH and =O) giving rise to two separated O(1s) features. It is this intermediate O(1s) peak shift that we have attributed to the "bridged structure". There has been considerable discussion of the possibility of such bridged structures in

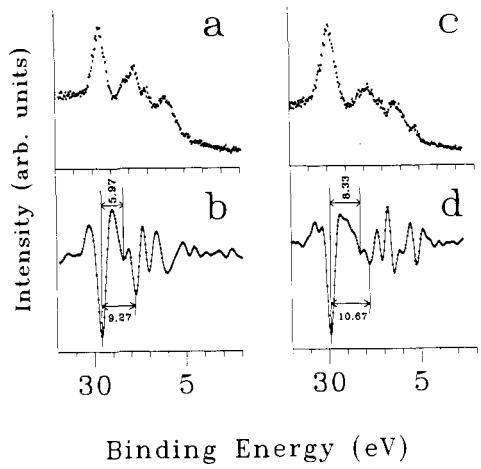

Figure 3. Valence-band XPS spectra of solid samples condensed onto a liquid nitrogen cooled sample probe: (a) hydroquinone, (b) second-derivative spectrum of (a); (c) benzoquinone, (d) second-derivative spectrum of (c).

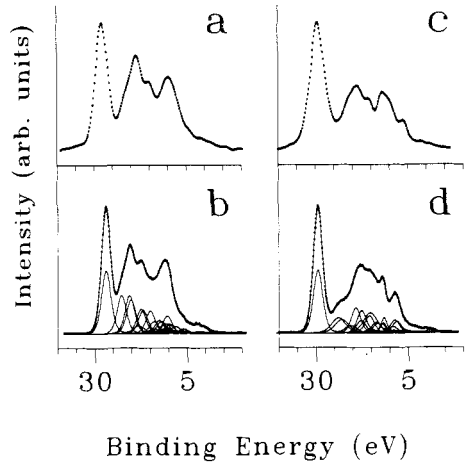

Figure 4. Valence-band XPS spectra of various samples compared with spectra calculated from Xα calculations: (a) hydroquinone as in Figure 3 with a nonlinear background removed; (b) calculated hydroquinone spectrum; (c) benzoquinone as in Figure 3 with a nonlinear background removed; (d) calculated benzoquinone spectrum.

acetylacetone (see, for example, ref 18 and references therein). In acetylacetone various possibilities exist including a "bridged structure". While the situation is clearly complex, possibly involving a double potential well, we regard the "bridged structure" as a reasonable model for this type of oxidation.

It is interesting to compare the O(2s)–C(2s) separation in the compounds quinone and hydroquinone. If our substituted coronene predictions are correct, then we should find a greater separation in quinone than in hydroquinone, and this is also predicted in our Xα calculations on these molecules (1.76 eV in our calculations). Figure 3 shows the original valence band data for these two molecules together with their second-derivative spectra. The second derivative spectra show the first C(2s) features to be separated by 5.97 and 8.33 eV, respectively (a 2.36-eV difference) in the two molecules. Figure 4 compares the nonlinear background subtracted and smoothed spectra with the calculated spectra. The agreement is especially good for hydroquinone. Despite similarities between the two experimental spectra, the experimental spectra differ

(18) Clark, D. T.; Harrison, A. *J. Electron. Spectrosc.* **1981**, *23*, 39.

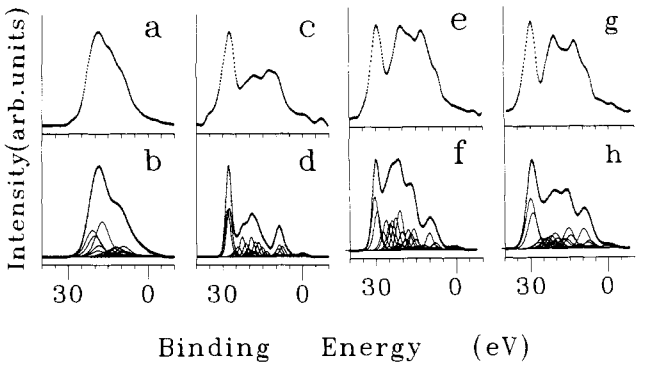

Figure 5. Valence-band XPS spectra of various carbon fiber samples compared with spectra calculated from Xα calculations. All experimental spectra were smoothed and had a nonlinear background subtracted: (a) untreated E-120 carbon fiber; (b) calculated untreated fiber spectrum based upon the model compound coronene; (c) anodically oxidized E-120 carbon fiber (2.0 V (SCE) for 20 min); (d) calculated spectrum based upon the hydroxide-group-substituted coronene model compound; (e) anodically oxidized E-120 carbon fiber (2.5 V (SCE) for 20 min); (f) calculated spectrum based upon hydrogen-bridged substituted coronene model compound; (g) anodically oxidized E-120 carbon fiber (3.0 V (SCE) for 20 min); (h) calculated spectrum based upon hydrogen-bridged substituted coronene model compound. The O(2s) and O(2p) cross sections in the calculated spectra were adjusted by a factor of 0.5 in (d), 0.1 in (f), and 0.5 in (h).

notably in that quinone has an additional feature at lowest binding energy, clearly predicted in our calculated quinone spectrum, and the binding energy of the O(2s) feature is at 30 eV in quinone and 28 eV in hydroquinone, again predicted in our calculated spectrum.

The O(2s)–C(2s) separation in ether type linkages, which is predicted by the calculations to be large, is indeed found to be large in previous studies of polymers. Thus the spectra of linear polyethers[19] show separations of the order 10 eV.

In comparing our calculated spectra for substituted coronenes with experimental spectra, we need to note that typically the oxygen-to-carbon ratio will be smaller than for the model compounds. The high oxygen-to-carbon ratio for the model compounds was chosen to give highly symmetric molecules and thus easier calculations. To adjust for a lowered oxygen-to-carbon ratio, we have adjusted the O(2s) and O(2p) photoelectron cross sections in generating the calculated spectra. Also the inclusion of the X-ray satellite features can make a significant contribution to the spectrum, a point that we missed in our earlier paper.[10] Thus the calculated spectrum for coronene shows more intensity at lower kinetic energy when this is done (compare Figure 5b with Figure 6b in ref 10), and this gives good agreement with the valence-band spectrum of a Du Pont E120 pitch-based carbon fiber (Figure 5a).

Figure 5 shows how the calculated spectra for the substituted coronenes compare with oxidized carbon fibers. The fiber oxidized in nitric acid at 2.0 V vs SCE (Figure 5c) gives a valence-band spectrum that can be well explained by $C_{24}O_{12}H_{12}$–the hydroxide-functionalized coronene. To account for a lower oxygen-to-carbon ratio, this calculated spectrum was adjusted so that the O(2s) and O(2p) cross sections were reduced to 0.5 of their normal value. The fibers oxidized to 2.5 V vs SCE (Figure 5e) and 3.0 V vs SCE (Figure 5g) give valence-band spectra that

(19) Pireaux, J. J.; Riga, J.; Caudano, R.; Verbist, J. *Photon, Electron and Ion Probes of Polymer Structure and Properties*; Dwight, D. W., Fabish, T. J., Thomas H. R., Eds.; ACS Symposium Series No. 162; American Chemical Society: Washington, D.C., 1981; p 169.

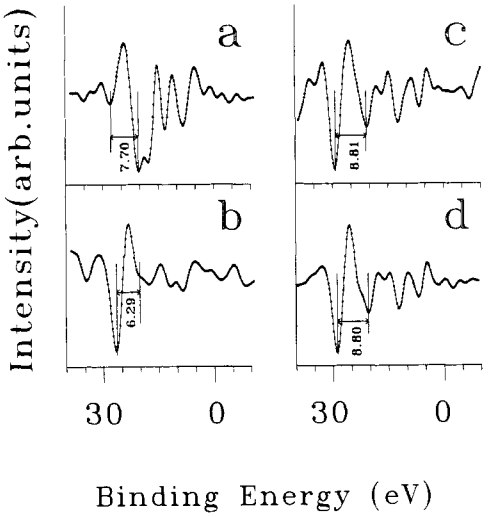

Figure 6. Second derivative of the valence-band XPS spectra of various carbon fiber samples: (a) untreated E-120 carbon fiber; (b) anodically oxidized E-120 carbon fiber (2.0 V (SCE) for 20 min); (c) anodically oxidized E-120 carbon fiber (2.5 V (SCE) for 20 min); (d) anodically oxidized E-120 carbon fiber (3.0 V (SCE) for 20 min).

can be well explained by the "bridged" structure $C_{24}O_{12}H_6$. The calculated spectra in Figure 5f,h were constructed with the O(2s) and O(2p) cross sections reduced to 0.1 and 0.5 of their normal values, respectively, to account for the increased oxygen-to-carbon ratio in the sample oxidized at 3.0 V vs SCE. Good overall agreement between the experimental and calculated spectra are obtained. Figure 6 shows the second-derivative spectrum for the four experimental spectra in Figure 5a,c,e,g (Figure 6a–d). The untreated fiber has only a very small O(2s) feature. The separations in the second-derivative spectra, 6.29 (2.0 V vs SCE) and 8.80 eV (3.0 V vs SCE) show an increasing separation with oxidation consistent with our assignment of the surface functionality to hyroxide at 2.0 V and the "bridged structure" at 2.5 and 3.0 V. Thus Figure 6b shows a clear shoulder at a separation of 6.29 eV, and this shoulder is predicted at a similar separation in the calculated hydroxide spectrum (Figure 5c). The shoulder is not seen in the calculated spectrum for the "bridged structure" (Figure 5h). The weak shoulder on the spectrum in Figure 6d to smaller separation (6.45 eV) may be caused by reduction of oxide to hydroxide in the instrument (decomposition in the XPS instrument is discussed elsewhere[12,13]).

We have already discussed above that the region below 18-eV binding energy might have a distinct "signature". We can show this theoretically by generating spectra for the same model molecule but with different O(2s) and O(2p) cross sections. When we do this, the peaks in the region below 18 eV shift in position and intensity. This is because these features are not due to one energy level but rather an overlap of different energy levels that combine to form peaks. We can show this experimentally by examining the spectra of fibers oxidized to different potentials, when we again see considerable variations in the peaks and features below 18 eV. Obviously the exact determination of the features below 18 eV provides a severe test for any calculations, but the suggestion that these features may vary both with the amount of a given functional group as well as with a change in the type of functional group seems reasonable.

Conclusions

The valence-band region of carbon fibers can be seen, from both experimental methods where the fibers are

oxidized and from calculations, to be highly sensitive to surface chemical functionality. Oxidized carbon is likely to show a greater variation in the O(2s) region than in many other oxygen-containing materials since the C(2s) energy is close to that of the O(2s) energy, and thus considerable mixing can occur between these two levels leading to significant chemical shifts. This situation is in contrast with the case of metal oxides where the O(2s) region is more corelike in its behavior.[20]

In general the valence-band region provides a more sensitive monitor of changes in surface chemistry than the core region. Thus changes in surface functionality result in significant differences (including in some cases separately resolved peaks) in the O(2s) region, as well as in the region at binding energies below 18 eV. In particular it can be seen that the calculations suggest that both the O(2s) binding energy and its separation from the C(2s) region provide analytical information allowing distinctions to be made regarding surface functionality. A striking example of the sensitivity of the valence-band region is in its predicted ability to distinguish between ether or epoxide type groups and hydroxide groups—groups that occur at a similar binding energy in the O(1s) core region. The valence-band region clearly has considerable potential as an analytical probe, one whose utility can be greatly assisted by accompanying calculations.

Acknowledgment. We are grateful to the Fibers Department of the Du Pont Co. for supporting this work and to the Department of Defense for providing funding for the X-ray diffraction equipment.

Registry No. Hydroquinone, 123-31-9; benzoquinone, 106-51-4; coronene, 191-07-1.

(20) Welsh, I. D.; Sherwood, P. M. A. *Phys. Rev. B* **1989**, *40*, 6386.

Semiconductor Particulate Films on Solid Supports

Xiao Kang Zhao and Janos H. Fendler*

Department of Chemistry, Syracuse University, Syracuse, New York 13244-4100

Received July 25, 1990

CdS and ZnS semiconductor particulate films, prepared in negatively charged monolayer interfaces and transferred to solid supports, have been characterized by reflectivity, absorption spectrophotometry, transmission electron microscopy, scanning tunneling microscopy, and electrical measurements. Incident-angle-dependent reflectivity measurements established the optical thicknesses of the semiconductor particulate films on solid supports to be only 5% smaller than those determined at the monolayer interfaces prior to their transfer. Absorption spectra of CdS and ZnS particulate films on quartz supports showed maxima around 239 and 200 nm and shoulders around 475 and 315 nm, respectively. Plots of absorbances at a given wavelength against thickness were linear for CdS and ZnS particulate films. Direct bandgaps for 63-, 125-, 163-, 204-, 263-, and 298-Å-thick CdS particulate films were evaluated to be 2.54, 2.48, 2.46, 2.44, 2.43, and 2.42 eV. Similarly, a direct bandgap of 3.75 eV was assessed for the 458-Å-thick ZnS particulate film. Heating of the CdS and ZnS films to 300–500 °C shifted the direct bandgaps to those corresponding to bulk semiconductors. Transmission electron micrographs of CdS films revealed the presence of CdS particles in a narrow size distribution with average diameters of 47 Å. The presence of 20–30-Å-thick, 40–50-Å-diameter CdS and 10–25-Å-thick, 30–40-Å-diameter ZnS particles in CdS and ZnS films were discerned by scanning tunneling microscopy. CdS films had dark resistivities of (3–6) × 10^7 Ω cm, which decreased upon illumination; they also developed photovoltages upon illumination. The action spectrum of the photoconductivity corresponded to the absorption spectrum of the CdS particulate film, indicating its origin to be the conduction band electrons and valence band holes produced in bandgap excitation.

Introduction

The altered mechanical, chemical, electrochemical, electrooptical, and magnetic properties that accompany size and dimensionality reductions have prompted the intensive investigation of nanosized particles and clusters.[1-3] In our laboratories, nanosized colloidal particles have been in situ generated and stabilized in such organized surfactant aggregates as reversed micelles,[4] surfactant and polymerized surfactant vesicles,[5-11] bilayer lipid membranes (BLMs),[12-14] and Langmuir–Blodgett (LB) films.[15,16] More recently, we reported that semiconductor particles could be in situ formed at monolayer interfaces. In particular, monolayers prepared from negatively charged arachidic acid (AA), bovine brain phosphatidylserine (PS), and *n*-hexadecyl-(4-vinylbenzamido)undecyl hydrogen phosphate (1) have been shown to attract cadmium and zinc ions and to act as templates for the in situ generation of semiconductor particles.[17] Controlled infusion of hydrogen sulfide resulted in the formation of covalent metal sulfide bonds at a large number of sites at

(1) Henglein, A. *Top. Curr. Chem.* **1988**, *143*, 113. Brus, L. A. *J. Phys. Chem.* **1986**, *90*, 2555. Andres, R. P.; Averback, R. S.; Brown, W. L.; Brus, L. E.; Goddard, W. A.; Kaldor, A.; Louie, S. G.; Moskovits, M.; Percy, P. S.; Riley, S. J.; Siegel, R. W.; Spaepen, F.; Wang, Y. *J. Mater. Res.* **1989**, *4*, 704.
(2) Henglein, A. *Chem. Rev.* **1989**, *89*, 1861.
(3) Fendler, J. H. *Chem. Rev.* **1987**, *87*, 877.
(4) Meyer, M.; Wallberg, C.: Kurihara, K.; Fendler, J. H. *J. Chem. Soc., Chem. Commun.* **1984**, 90.
(5) Youn, H. C.; Tricot, Y.-M.; Fendler, J. H. *J. Phys. Chem.* **1985**, *89*, 1236.
(6) Tricot, Y.-M.; Fendler, J. H. *J. Am. Chem. Soc.* **1984**, *106*, 2475.
(7) Tricot, Y.-M.; Fendler, J. H. *J. Am. Chem. Soc.* **1984**, *106*, 7359.
(8) Rafaeloff, R.; Tricot, Y.-M.; Nome, F.; Fendler, J. H. *J. Phys. Chem.* **1985**, *89*, 533.
(9) Rafaeloff, R.; Tricot, Y.-M.; Nome, F.; Tundo, P.; Fendler, J. H. *J. Phys. Chem.* **1985**, *89*, 1236.
(10) Tricot, Y.-M.; Emeren, Å.; Fendler, J. H. *J. Phys. Chem.* **1985**, *89*, 4721.
(11) Tricot, Y.-M.; Fendler, J. H. *J. Phys. Chem.* **1986**, *90*, 3369.
(12) Deleted in proof.
(13) Baral, S.; Fendler, J. H. *J. Am. Chem. Soc.* **1989**, *111*, 1604.
(14) Zhao, X. K.; Baral, S.; Fendler, J. H. *J. Phys. Chem.* **1990**, *94*, 2043.
(15) Xu, S.; Zhao, X. K.; Fendler, J. H. *Adv. Mater.* **1990**, *2*, 183.
(16) Yi, K. C.; Fendler, J. H. *Langmuir*, in press.
(17) Zhao, X. K.; Xu, S. Q.; Fendler, J. H. *Langmuir*, submitted for publication.

0897-4756/91/2803-0168$02.50/0